Electronic Supplementary Material (ESI) for Lab on a Chip.

Supplementary Information

Vacuum pouch microfluidic system and its application for thin-film micromixer

CHENG-JE LEE AND YU-HSIANG HSU*

Institute of Applied Mechanics, National Taiwan University, No. 1, Sec.4, Roosevelt Rd., Taipei 10617, Taiwan (R.O.C).

**yhhsu@iam.ntu.edu.tw.*

FINITE ELEMENT ANALYSIS AND EXPERIMENTAL STUDY OF THE SERPENTINE MICROMIXER

The finite element analysis (FEA) of the serpentine micromixer was conducted using the COMSOL Multiphysics® software. The micromixer first was built inside the software, and incompressible Navier-Stokes equation was used to model the flow behaviour inside the serpentine channel. Nine different levels of volume flow rate were set equally at the two entrances to study the mixing mechanism. The resulting volume flow rate *Q* in the serpentine micromixer was 1, 2.5, 5, 10, 20, 50, 100, 200 and 500 µl/min. The exit of the micromixer was set at 0 Pa, and non-slip boundary condition was set on all other surfaces. The density and dynamic viscosity of reagents were 1 kg m-3 and 1 cP, respectively. The flow pattern was traced by simulated streamline. FEA results were compared with trajectories of red-fluorescent 1 µm polystyrene beads (Sigma-aldrich L2778) flowed inside a PDMS molded serpentine micromixer driven by two syringe pumps. The correlations between the flow pattern and mixing performance were studied, and the dependency on Reynolds number also was investigated. The mixing performance also was simulated using time-dependent analysis. The diffusivities of food dye and fluorescein solution (Sigma-Aldrich F6377) measured by the Y-shape mixing channel was used for finite element analysis, and mixing performance was studied under different volume flow rates and Reynolds numbers.

FINITE ELEMENT ANALYSIS OF THE SERPENTINE MIXER

Figure S1 shows FEA results of the serpentine micromixer. Simulated streamlines of three different levels of volume flow rates at 1 µl/min (Re=0.13), 10 µl/min (Re=1.33) and 500 µl/min (Re=66.67) are shown in Figs. S1(C1), S1(B1) and S1(C1), respectively. It shows that, at high flow rate, a vortex can occur at corners with right angles [Fig. S1(C1)] and fluidic flow can become chaotic, as demonstrated in previous reports [R1-R2]. In contrast, streamlines did not cross each other at lower flow rates [Figs. S1(A1) and S1(B1)]. To experimentally visualize flow profiles under different flow rates, 1 µm red fluorescent Polystyrene (PS) beads were suspended in DI-water and pumped into PDMS micromixer to mix with DI-water by two syringe pumps. Figures S1(A2), S1(B2) and S1(C2) show captured trajectories of PS beads. These images were inverted to make PS beads easy to trace. It shows that PS beads flow smoothly along the serpentine micromixer at 1 µl/min [Fig. S1(A2)] and 10 µl/min [Fig. S1(B2)], but not for 500 µl/min [Fig. S1(C2)]. Localized vortices were observed clearly at corners (black arrow) of the serpentine channel at high Reynolds numbers [Fig.

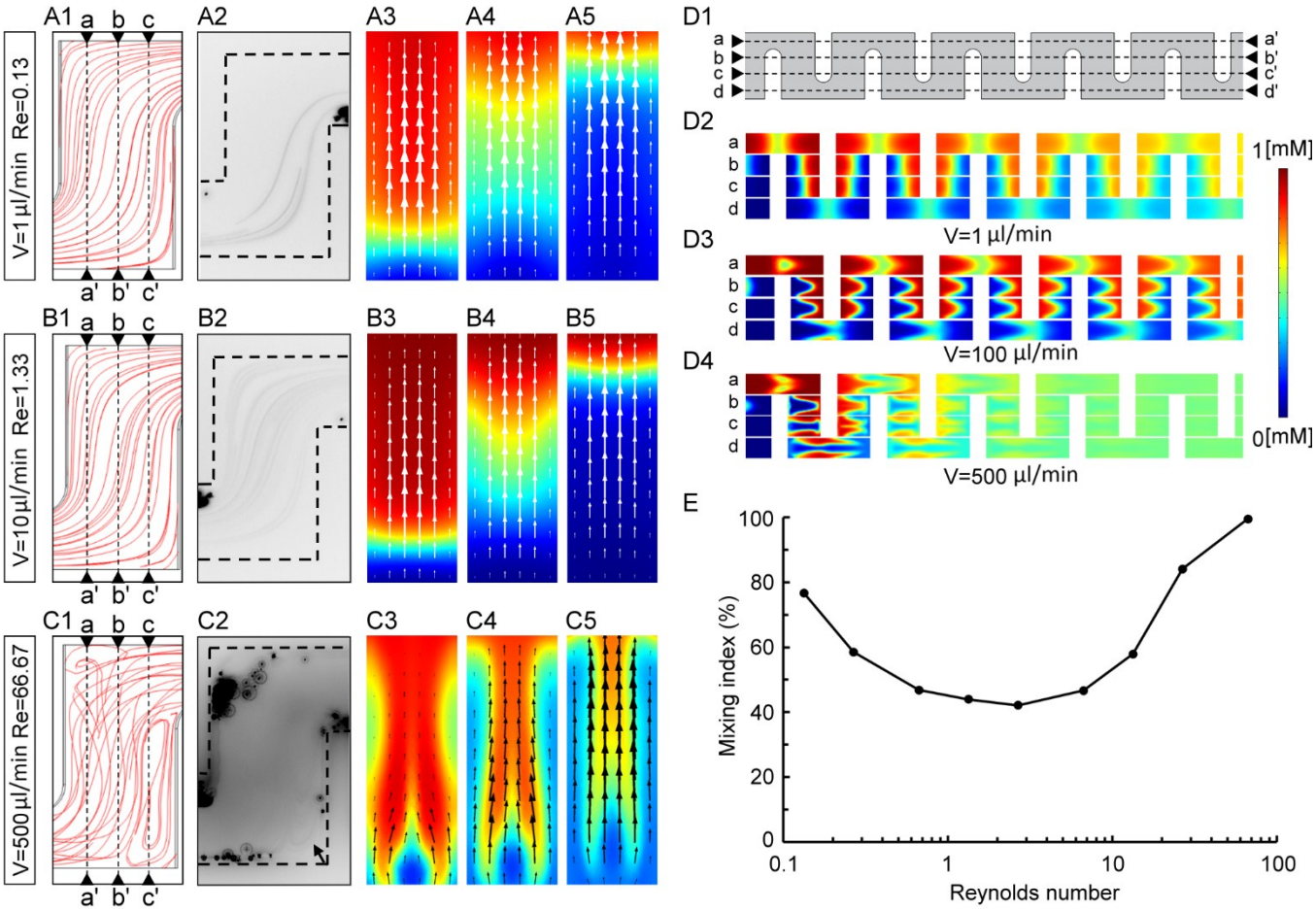

Fig. S1 Images of FEA results and experimental results under conditions of 1 µl/min (A1-A5), 10 µl/min (B1-B5) and 500 µl/min (C1-C5), where (A1, B1 and C1) are streamlines and (A2, B2 and C2) are trajectories of traced fluorescent beads. The corresponding concentration distributions (colors) and velocity vectors (arrows) for each condition on the a-a' (A3, B3 and C3), b-b' (A4, B4 and C4) and c-c' (A5, B5 and C) cross-sections are included. (D1-D4) Simulated concentration profiles along 10 obstacles of a serpentine micromixer on 4 cross-sections (D1) and three different flow rates, including 1 µl/min (D2), 100 µl/min (D3) and 500 µl/min (D4). (E) Simulated dependency of mixing index on Reynolds number.

S1(C2)]. This induction of chaotic vortex contributed to the mixing process in the range of high flow rates, whereas diffusion contributed mainly at low flow rates. This effect was investigated further by comparing the cross-sectional flow pattern on a-a', b-b' and c-c' plan in Figs. S1(A1),S1(B1) and S1(C1), and the simulated results are shown in Figs. S1(A3-A5), S1(B3-B5) and S1(C3-C5), respectively. Concentration distributions are demonstrated in color, and velocity vectors are indicated by arrows. This result demonstrated that the direction of fluidic flow can be altered at high flow rate [Fig. S1(C3-C5)] but not at low flow rates [Figs. S1(A3-A5) and S1(C3-C5)].

To understand the mixing efficiency, the patterns of molecules mixed along the serpentine micromixer were simulated and compared. Figure S1(D1) shows the 4 cross-sectional surfaces studied. Figure S1(D2), S1(D3) and S1(D4) show FEA results at 1 µl/min (Re=0.13), 100 µl/min (Re=13.33) and 500 µl/min (Re=66.67), respectively. Figure S1(D2) demonstrates that diffusion is the dominant mass transport at low flow rate and Re number. It also shows molecules diffused laterally along the serpentine channel. On the other hand, folding and rotation are observed at high flow rates and Re number [Figs. S1(D3) and S1(D4)], verifying that chaotic advection is the dominant mechanism. Figure S1(E) summarizes the correlation between mixing index and Re number by analysing FEA results. It shows that the mixing index of the serpentine micromixer has a biphasic correlation with Re number. In summary, FEA results suggest that

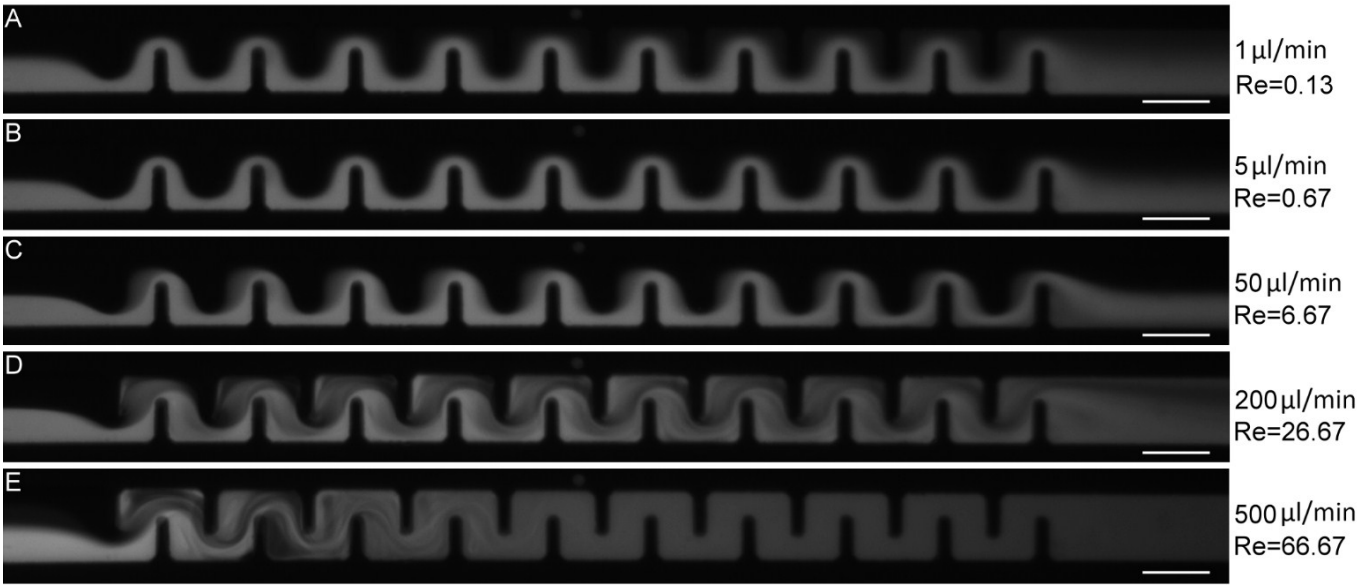

Fig. S2 Mixing micrographs of 5µg/ml FITC fluoresce solution and DI-water in PDMS micromixers with 20 obstacles, where the volume flow rates are 1µl/min (A), 5µl/min (B), 50µl/min (C), 200µl/min (D) and 500µl/min (E). (Scale bar = 200µm)

diffusion dominates at very low flow rate since it provides sufficient time for lateral mixing. At high flow rate, chaotic advection promotes mixing efficiency, whereas intermediate flow rate and Re number has the lowest mixing index.

EXPERIMENTAL STUDY ON THE MIXING MECHANISM AND THE DEPENDENCY OF REYNOLDS NUMBER

To verify the mixing mechanism experimentally, PDMS micromixers with 10 and 20 obstacles were investigated and two syringe pumps were used to control flow rates. Figure S2(A) to S2(E) show mixing patterns of the PDMS micromixer with 20 obstacles under 5 levels of volume flow rates and Re numbers. Fluorescein solution and DI-water were used in this study. It was verified that diffusion dominated the mixing mechanism at low Re number [Figs. S2(A)-S2(B)], and the mixing was more complete at lowest flow rate [Fig. S2(A)]. In contrast, chaotic mixing can be observed at high volume flow rate and Re number [Figs. S2(D) and S2(E)], where folding and vortices can be observed. This suggests that chaotic advection dominates the mixing effect. This also demonstrated that chaotic mixing was more effective than diffusive mixing. At intermediate flow rate [Fig. S2(C)], the mixing efficiency was the least with a lower degree of folding effect.

The measured mixing indices for micromixers with 10 and 20 obstacles are shown in Figs. S3(A) and S3(B), respectively. The black dotted lines and gray dotted lines are results of fluorescein solution and food dye, respectively. The volume flow rate ranged from 1 µl/min to 500 µl/min, resulting in Re number ranging from 0.13 to 66.67. The biphasic distribution of mixing index with respect to Re number was evident for both cases, and micromixers with 20 obstacles had better mixing efficiency. Food dye also had better mixing results since its diffusion coefficient was 1.28 times higher. These findings verified the simulation results shown in Fig. S1(E). Note that the biphasic distribution of the food dye was not as smooth as the fluorescein solution. This effect could due to the food dye being composed of nanoparticles and not being dissolved in the DI-

water. Finally, it also demonstrated that this serpentine micromixer had lowest mixing efficiency at Re number in the range between 1 and 10 for both 10 and 20 obstacles.

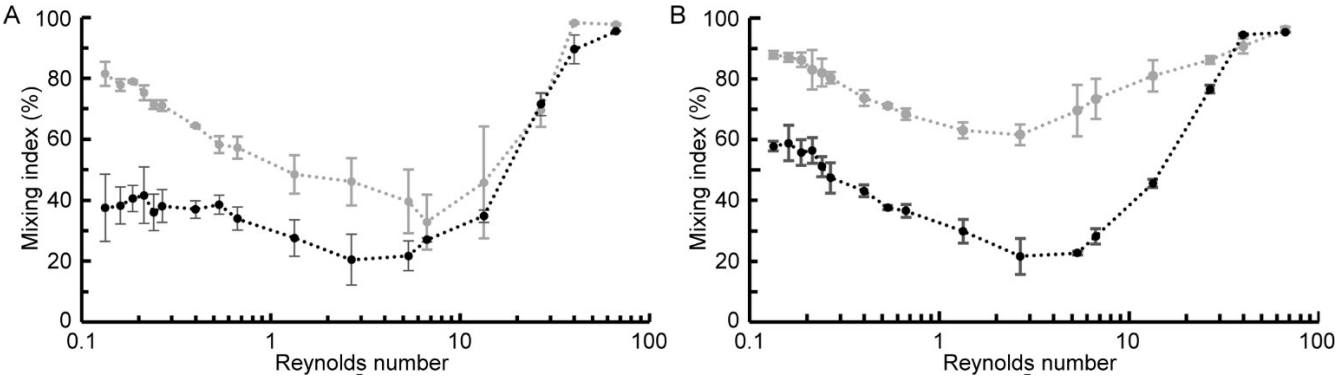

Fig. S3 Measured mixing index (MI) for PDMS micromixers with 10 (A) and 20 (B) obstacles, where black dotted lines and gray dotted lines are results of fluorescein solution and food dye, respectively.

Supplementary Reference

R1. S. Hossain, K.-Y. Kim, Micromachines 2015, 6, 842-854. (doi:10.3390/mi6070842)

R2. K.W. Oh, K. Lee, B. Ahn and E.P. Furlani, Lab chip 2012, 12, 515. (doi:10.1039/c2lc20799k)